Title

Incidence and persistence of silver nanoparticles throughout the wastewater treatment process

Authors

Cervantes-Avilés, Pabel
Huang, Yuxiong
Keller, Arturo A

Publication Date

2019-06-01

DOI

10.1016/j.watres.2019.03.031

Peer reviewed

Water Research 156 (2019) 188–198

Contents lists available at ScienceDirect

Water Research

journal homepage: www.elsevier.com/locate/watres

Incidence and persistence of silver nanoparticles throughout the wastewater treatment process

Pabel Cervantes-Avilés [a, b, 1], Yuxiong Huang [a, b, c, 1], Arturo A. Keller [a, b, *]

[a] Bren School of Environmental Science and Management, University of California, Santa Barbara, CA, 93106, USA
[b] Center for Environmental Implications of Nanotechnology, University of California, Santa Barbara, CA 93106, USA
[c] Shenzhen Environmental Science and New Energy Technology Engineering Laboratory, Tsinghua-Berkeley Shenzhen Institute, Shenzhen 518055, PR China

ARTICLE INFO

Article history:
Received 29 January 2019
Received in revised form
14 March 2019
Accepted 16 March 2019
Available online 20 March 2019

Keywords:
Ag NPs
Single particle ICP-MS
Dissolution
Stability
Fate of nanomaterials
Mass flow of nanoparticles

ABSTRACT

While the predicted or observed concentrations of Ag NPs in wastewater treatment plants (WWTPs) have ranged from μg/L to ng/L, there is still uncertainty with regards to the realistic concentration range of Ag NPs in WWTPs. In addition, the persistence, removal, and size of Ag NPs throughout WWTP process is also not well investigated, particularly in real operating conditions. In this study, the incidence and persistence of Ag NPs in the wastewater process were studied by using single particle inductively coupled plasma mass spectrometry (sp-ICP-MS). The incidence of Ag NPs was determined in samples collected at the influent and effluent of the conventional process, as well as reclaimed and backwash waters of the ultrafiltration (UF) system in a WWTP (Santa Barbara, CA), showing a concentration of 13.5, 3.2, 0.5 and 9.8 ng/L, respectively, with relative standard deviations (RSDs) < 5%. Total Ag concentration (Ag NP and Ag^+) ranged from 40 to 70 ng/L, in line with lower predicted values. Most of the Ag NPs detected were below 100 nm, with a few above 100 nm in the conventional effluent. Biological and physical processes in the secondary treatment removed 76.3% of the colloidal Ag fraction, while with the tertiary treatment (UF) the WWTP achieved a removal of 96.3% of the colloidal fraction. Persistence of Ag NPs in various water matrixes, including a synthetic wastewater (SWW), was determined by spiking 300 ng/L of Ag NPs (40 nm) and monitoring the concentrations and size change for 15 days. The persistence of Ag NPs in suspension was Influent > Effluent > Reclaimed > SWW. Partial dissolution of NPs in all waters was observed from time 0 h. Although the current concentrations in the outlet flows from WWTP (effluent and reclaimed waters) were low, the presence of small and stable Ag NPs may raise ecotoxicological concerns via bioaccumulation.

1. Introduction

The growing use of nanoparticles (NPs) in consumer products has raised concerns about their potential impacts in the environment. The incidence of silver (Ag) NPs in wastewater is expected due to their incorporation and release from several product categories (Gottschalk et al., 2013; Hendren et al., 2013; Lazareva and Keller, 2014). Ag NPs are found in clothes (Impellitteri et al., 2009; Tulve et al., 2015), drinking water filters (Lalley et al., 2014), health care products and medical devices (Zhang et al., 2016b), personal care products (Echavarri-Bravo et al., 2017), and printable electronics (Shen et al., 2014). A certain amount of Ag NPs and Ag^+ are released from consumable products into wastewater and can arrive to the wastewater treatment plant (WWTP) (Impellitteri et al., 2009; Li et al., 2013), which is an important pathway for Ag NPs arriving to aquatic ecosystems (Lazareva and Keller, 2014; Liu et al., 2014; Musee, 2017). A fraction of singly dispersed Ag NPs with high colloidal stability may persist through the WWTP process and be released into the environment (Chinnapongse et al., 2011). Hence, detection and quantification of persistent Ag NPs in wastewater streams is key for evaluating their ecotoxicological implications (e.g., due to their antibacterial activity (Azimzada et al., 2017; Maurer-Jones et al., 2013)) at environmentally realistic concentrations (Holden et al., 2016).

Several studies have investigated the fate and effects of Ag NPs in WWTPs by spiking pristine NPs with concentrations from μg/L to

* Corresponding author. Bren School of Environmental Science and Management, 3420 Bren Hall, University of California, Santa Barbara, CA, 93106, USA.
E-mail address: keller@bren.ucsb.edu (A.A. Keller).
[1] P. C. and Y. H. contributed equally to this manuscript, considered as co-first authors.

https://doi.org/10.1016/j.watres.2019.03.031
0043-1354/

mg/L in lab scale experiments (Cao et al., 2018; Gottschalk et al., 2013; Kaegi et al., 2011; Ma et al., 2013a). The main receptor of Ag NPs in WWTPs is the waste sludge (and later the biosolids) from the removal of more than 90% of NPs from the water column (Kaegi et al., 2013; Ma et al., 2013b; Wang et al., 2016). Negative effects of Ag NPs in biological reactors have been observed at 0.05 mg/L Ag NPs (Choi and Hu, 2008), and include the inhibition of both, the nitrification process at 0.1 mg/L Ag NPs (Hou et al., 2012), and the denitrification processes at 2 and 5 mg/L Ag NPs (Zheng et al., 2018). It should be noted that these experimental concentrations were higher than those predicted for domestic wastewater (Lazareva and Keller, 2014; Sun et al., 2016). The fate and ecological implication of Ag NPs have a close relationship with the concentrations of NPs and dissolved silver ions in wastewater, time of exposure, and transformation of silver species (e.g., AgCl, Ag_2S, AgO) in the WWTP (Zhang et al., 2016b).

In wastewater, some of the soluble constituents have been shown to influence Ag NP stability (Doolette et al., 2013). The transformation of Ag NPs into Ag_2S in a sewer channel was studied by using extended X-ray absorption fine structure (EXAFS) techniques (Kaegi et al., 2013). Results showed the crystallization of Ag_2S and coarsening of an Ag_2S shell on the surface of the Ag NPs (Kaegi et al., 2013), making them less toxic that pristine Ag NPs (Clement Levard et al., 2013a). The interaction between Cl^- and Ag NPs in water results in the precipitation of $AgCl_{(s)}$, with a strong dependence on Cl/Ag molar ratios (Clément Levard et al., 2013b). Other potential transformations in the wastewater are the oxidation of Ag NPs to release Ag^+ and the reduction of Ag^+ to form new Ag NPs by dissolved organic matter (DOM), which could both happen in sunlit DOM-rich water (Yu et al., 2014).

Based on earlier modeling, the concentration of silver arriving at the WWTP was predicted to be in the 2–18 μg/L range (Blaser et al., 2008). In other studies, Ag NPs and their transformation products in the effluent of WWTPs have been predicted to be in the 3–260 ng/L range (Lazareva and Keller, 2014; Sun et al., 2016). Thus there is a substantial difference in estimates, of 3–4 orders of magnitude.

The half maximal effective concentration (EC_{50}) of Ag NPs in toxicological experiments ranges from 0.1 to 26 mg/L, where the most sensitive organism to Ag NPs was *D. magna*, followed by algae *P. subcapitata*, bacteria *E. coli* and *P. fluorescens*, yeast *S. cerevisiae*, and finally, mammalian fibroblasts *in vitro* (Ivask et al., 2014). Choi and Hu (2008) observed that the EC_{50} for nitrifying bacteria was 0.14 mg/L Ag NPs. Since EC_{50} concentrations are determined in spiked and controlled experiments, realistic concentrations of Ag NPs in WWTP effluent need to be determined in order to close the uncertainty in predictions and evaluate the ecotoxicological risk to aquatic ecosystems. Knowledge of the real influent concentrations is also needed to determine whether there is a risk to the microbial processes within the WWTP. Since previous studies have focused on the detection and quantification of Ag NPs in the effluent of WWTPs (Mitrano et al., 2012; Telgmann et al., 2014; Tuoriniemi et al., 2012), observed data on Ag NP concentrations in WWTP influent is still scarce. Given the substantial differences in concentrations of the water constituents (e.g. organic matter, suspended solids, dissolved salts, etc.) between influent and effluent, there could be some interference on the detection and quantification of Ag NPs. Hence, determining the incidence of Ag NPs in the influent, and later persistence in the wastewater flow throughout the WWTP may pose a challenge.

The current direct methods for measuring NP concentrations in complex media include imaging and spectroscopy techniques, which have some limitations such as detection limits, matrix interferences, and speciation (Laborda et al., 2016). These issues have led researchers to measure the concentrations using different techniques and approaches (McGillicuddy et al., 2017). Scanning and transmission electron microscopy (SEM and TEM, respectively) have been used to confirm the presence of NPs in wastewater, as well as characterize their morphology (Cervantes-Avilés et al., 2017; Doolette et al., 2013). However, image acquisition of NPs in WWTP and environmental samples is labor intense, and may be biased particularly at environmentally realistic concentrations, since it may be difficult to locate a truly representative region. SEM or TEM in tandem with element-selective detection techniques, such as inductively coupled plasma mass spectrometry (ICP-MS), ICP-optical emission spectrometry (ICP-OES) (or ICP-atomic emission spectrometry (ICP-AES)) are the most commonly employed techniques for elemental quantification of inorganic NPs in wastewater (Choi et al., 2017; Kaegi et al., 2013; Laborda et al., 2016; Park et al., 2013). However, the information is generally limited to only total concentration, combining the concentrations of both NPs and dissolved ions (Kaegi et al., 2013; Ma et al., 2013a). In order to use ICP to measure the concentration of NPs only, pretreatments, for example, ultrafiltration (Choi et al., 2017; Laborda et al., 2016), cloud point extraction (CPE) and ionic exchange resin (IER) (Chao et al., 2011; Hadioui et al., 2014; Li et al., 2013) have been applied to remove the metal ions. Nonetheless, NP recovery efficiency depends on water characteristics and NP coating (Li et al., 2012). Another approach to detect Ag NPs has been surface-enhanced Raman scattering (SERS). In this technique, Raman signals are enhanced by indicator molecules bound to the Ag NPs; the signals exhibit a linear relation at mg/L concentrations (Guo et al., 2016). However, at the predicted concentrations of Ag NPs (μg/L and below), there are interferences in the Raman signal due to matrix components (Guo et al., 2016). Therefore, emerging analytical techniques that can quantify NPs in wastewater at realistic concentrations with low detection limits are needed.

Single particle ICP-MS (sp-ICP-MS) is a novel technique able to quantify the number concentration of NPs in suspension, as well as the elemental mass per nanoparticle by measuring "particle by particle" (Laborda et al., 2016, 2014; Montaño et al., 2014). sp-ICP-MS has been applied to quantify and characterize TiO_2 NPs in cosmetics (de la Calle et al., 2017), Ag NPs in antimicrobial products (Cascio et al., 2015), TiO_2, Au and Ag NPs in drinking water (Donovan et al., 2016) and Cu NPs in biological tissues (Keller et al., 2018). sp-ICP-MS has also been used to determine Ag NP concentration in spiked mesocosms (Tuoriniemi et al., 2017) and in lake samples (Aznar et al., 2017; Wimmer et al., 2018). In another study, Ag NPs were spiked into two wastewater samples, with no background Ag, at concentrations of 100 ng/L (influent) and 200 ng/L (effluent), to evaluate the performance of an sp-ICP-MS (Mitrano et al., 2012). However, the study did not provide information on the presence of Ag NPs in an operating WWTP, their size distribution, their persistence or the removal efficiency at various stages of the treatment; this information is important for modeling studies. Other studies have evaluated the size of spiked Ag NPs in wastewater influent and effluent using sp-ICP-MS (Telgmann et al., 2014; Tuoriniemi et al., 2012), but the incidental mass concentrations and removal of Ag NPs in WWTPs were not determined. Hence, research is needed to determine realistic influent and effluent concentrations of Ag NPs in WWTPs, as well as their size distribution and persistence in these complex media. As stated above, the key advantages of sp-ICP-MS include elemental selectivity, low detection limits, direct and simultaneous measurement of ionic and NP concentrations, and NPs size distribution (Aznar et al., 2017; Laborda et al., 2016), making it a suitable method for the analysis of environmental samples, including different locations within the WWTP.

In this work, we first calibrated the sp-ICP-MS to quantify and size the Ag NPs, in DI water, citrate buffer and synthetic wastewater (SWW); this serves to determine the importance of the matrix in

the calibration process. Then, we investigated the incidence and persistence of Ag NPs at different locations within an operating WWTP, including influent, secondary effluent, tertiary reclaimed water and backwash water. The persistence of Ag NPs was studied over time in the different stages of wastewater treatment, and in SWW. Understanding the influent and effluent concentrations of Ag NPs, as well as their persistence, can help to better assess their risk to the WWTP processes and the environment.

2. Methods and materials

2.1. Sampling and characterization of wastewater

Wastewater samples were collected in El Estero WWTP at Santa Barbara, California. Sampling points were primary clarifier (influent pipe port), top of the secondary clarifier, tertiary ultrafiltration (UF) system with 0.1 μm of pore size (pipe port) and the retentate of the UF (pipe port). Samples were labeled as influent, effluent, reclaimed and backwash water, respectively. Sampling points are indicated in the diagram presented in the Supplementary material (Fig. S1). Polyethylene containers (1 L) with polypropylene caps were submerged in nitric acid (10%) overnight before the sampling day. On site, containers were rinsed three times with the respective wastewater samples before they were filled, and samples were stored 20 h at 4 °C until the next day for analysis by sp-ICP-MS and physicochemical characterization.

Characterization of wastewater samples consisted of determining per triplicate the concentration of organic matter as carbohydrates, nitrogen species, orthophosphate, and suspended solids. Dissolved carbohydrates (DC) content was determined with the phenol-sulphuric acid method (Nielsen, 2010), using glucose as a standard. Total nitrogen (TN), ammonia (NH_4^+), nitrate (NO_3^-), nitrite (NO_2^-), orthophosphate (PO_4^{3-}) and sulfide (S^{2-}) were measured by colorimetric tests (Hach DR 890, HACH Company). Total, fixed and volatile suspended solids (TSS, FSS, and VSS, respectively) were determined according to standard methods (APHA, 2005). Ionic strength (IS) was calculated from measured electrical conductivity (Zetasizer Nano ZS90, Malvern Panalytical Ltd) using Equation (1) (Ponnamperuma et al., 1966):

$$IS = Elec.Conductivity(\mu S/cm) \bullet 1.6 \times 10^{-5}\ (\text{in equivalents/L}) \quad (1)$$

2.2. Silver nanoparticles (Ag NPs)

For the persistence studies, a stock aqueous suspension (0.02 mg/mL) of Ag NPs capped with polyvinylpyrrolidone (PVP), with a nominal size of 40 nm was purchased from Sigma-Aldrich. Mean size was confirmed as 42 ± 25 nm using NanoTracking Analysis (Fig. S2) (NTA, NanoSight LM10, Malvern Panalytical Ltd.). See supplementary material file for details about operating conditions (Table S2) and completed tracks and frames considered (Table. S3). The plasmon resonance excitation was determined by scanning the UV–vis peak (UV, 1800; Shimadzu), and it corresponded to 414 nm (Fig. S3). The zeta potential (ZP) of Ag NPs was −14.7 ± 1.6, and it was determined in DI water at a pH of 6.75 by Laser Doppler Velocimetry (Zetasizer Nano ZS90, Malvern Panalytical Ltd).

2.3. sp-ICP-MS measurement

The concentration and size of the Ag NPs were determined using an Agilent 7900 ICP-MS (Santa Clara, CA, USA) with an sp-ICP-MS module. The instrument was equipped with an autosampler and a standard peristaltic pump, standard glass concentric nebulizer, quartz spray chamber and quartz torch, standard nickel sampling and skimmer cones. Analyses were performed in time-resolved analysis (TRA) mode using an integration time (dwell time) of 100 μs per point with no settling time between measurements, similar to a previous study (Tuoriniemi et al., 2017). The instrument settings used for the sp-ICP-MS analysis are summarized in Table 1.

Table 1. Agilent 7900 sp-ICP-MS operating conditions.

The sp-ICP-MS method setup, data collection, and analysis were controlled via the Single Nanoparticle Application Module (method wizard) in the Agilent ICP-MS MassHunter software (Version C.01.03 Build 505.16 Patch 3). Ag NPs (60 nm in diameter) in 2 mM sodium citrate (NanoComposix Inc.) were used as reference particles. An aliquot of these particles was diluted from 500 to 1 ng/L with DI water in metal-free polypropylene tubes, to evaluate the nebulization efficiency and to be used for data conversion from raw signal to NP size. To ensure that the samples were fully homogenized, they were placed in an ultrasonic bath (Bransonic, Emerson) for 15 min at 280 W and a frequency of 40 kHz. An Ag ionic standard of 1 μg/L was prepared with 1% nitric acid and was used to determine the elemental response factor. The monitored analyte mass was ^{107}Ag. Silver particle density was set to 10.5 g/cm^3. Collected water samples were filtered through 0.45 μm pore size to avoid the sampler cone blockage caused by suspended solids (Tuoriniemi et al., 2017). Nitrocellulose filters were used due to high affinity with microorganisms and large debris present in wastewater. Filtrates were analyzed in triplicate without dilution.

2.4. Persistence of Ag NPs in wastewater experiments

To study the persistence of Ag NPs and Ag^+ in wastewater, Ag NPs were spiked into influent, effluent, reclaimed water, and SWW. SWW was included in the experiment since it is frequently used for NP ecotoxicological studies in wastewater (Gartiser et al., 2014; Tan et al., 2015). SWW was prepared based on a previous study (Cuevas-Rodríguez et al., 2015). In brief, SWW contained 380.4 mg/L of D-glucose, 45.1 mg/L NH_4OH, 14.4 mg/L K_2HPO_4, 14.2 mg/L NaCl, 8.8 mg/L $MgSO_4 \cdot 7H_2O$ and 3.8 mg/L $CaCl_2 \cdot 2H_2O$. All wastewater matrixes were filtered with 0.45 μm nitrocellulose filter papers before being spiked with Ag NPs, to prevent blockage of the sampler cone due to the suspended solids (Tuoriniemi et al., 2017). After filtration, aliquots (0.5 L) of each wastewater were transferred to borosilicate bottles. The wastewater samples were spiked with Ag NPs (40 nm) to achieve a nominal 300 ng/L, and then vortexed 5 s at 3200 rpm. The bottles were covered with aluminum foil and left to stand for 15 days. Samples were collected 3 cm below the surface after the first 14 h. Samples were then collected from the same position every 24 h up to 374 h. Samples were stored at 4 °C in metal-free polypropylene tubes until analysis by sp-ICP-MS. Size and concentration of Ag NPs, as well as Ag^+ concentration in wastewater were determined by sp-ICP-MS analysis in all collected samples. ZP of the Ag NPs in wastewater matrixes was measured

Table 1
Agilent 7900 sp-ICP-MS operating conditions.

Parameter	Operation Setting
Reference material	100 ng/L Ag NPs 60 nm
RF power	1550 W
Carrier gas flow	0.67 L/min
Nebulizer pump velocity	0.1 revolutions per s
Acquisition time	60 s
Dwell time	100 μs
Mass monitored	^{107}Ag

(Zetasizer Nano ZS90) at initial and final time (0 and 374 h) in order to study their stability. Bottles were vortexed 5 s at 3200 rpm at the end of the experiment, to resuspend the particles for ZP determination. Additionally, the surface charge at different pH and isoelectric point (IEP) of Ag NPs (100 μg/L) was determined (Zetasizer Nano ZS90) in all wastewaters by auto-titration with 0.1 M HNO_3 and 0.1 M NaOH (MPT-2, Malvern Panalytical Ltd).

3. Results and discussion

3.1. Wastewater characteristics

The results indicated a significant removal of soluble carbon and soluble forms of nitrogen, such as NH_4^+, NO_2, and NO_3 during the wastewater treatment process (Table 2), going from influent to secondary effluent and then tertiary reclaimed water (Fig. S1). Note that the sum of NH_4–N, NO_3–N, and NO_2–N are often significantly larger than the TN concentrations.

In the backwash water from the filtration process, the concentrations of both C and N were similar to the secondary effluent. PO_4–P in the effluent decreased significantly after the anoxic-aerobic conditions in the secondary treatment, due to the accumulation of PO_4–P in organisms present in the biological processes (Chan et al., 2017). The concentration of PO_4–P remained almost constant from the effluent to reclaimed water as well as in the backwash water. SWW had the highest dissolved carbon, while TN and PO_4–P were close to El Estero effluent values.

Previous studies have indicated that pH and IS can affect the stability of Ag NPs in suspension (Zhang et al., 2016a). Both parameters remained relatively constant in the water streams of the WWTP, with a pH slightly above 7 and IS near 0.04 equiv/L (Table 2). The main characteristic that varied between the various water matrixes was the C:N:P ratios, which were calculated according to the elemental fraction of the measured parameters: dissolved C, NH_4^+, NO_3^-, NO_2^- and PO_4^{3-}. C:N:P ratios were 100:81:5 for influent, 100:69:3 for secondary effluent, 100:97:4 for tertiary reclaimed, 100:62:4 for backwash and 100:5:1 for SWW. This reflects the high removal of organic matter from influent to effluent. The C:N ratio in reclaimed water decreased due to the removal of organic colloids. These colloids led to the increase of the C:N ratio in the backwash water.

3.2. Calibration of sp-ICP-MS with Ag NPs in different water matrixes

The calibration curves of Ag NPs (60 nm) in different water matrixes, including 1 mM citrate buffer, SWW, and DI water were obtained by analyzing from 1 to 500 ng/L using sp-ICP-MS (Fig. 1). The calibration curves in all three water matrixes exhibited excellent linearity, with $R^2 > 0.99$ across the entire concentration range. However, the measured concentrations of Ag NPs in DI water were around 25% lower than nominal values (Fig. 1C), particularly at the higher concentration range (e.g., 200 and 500 ng/L). The lack of organic matter and dissolved ions in DI water may reduce the physical (e.g., electrostatic) and chemical (e.g., chelating, binding) interactions between Ag NPs and water constituents (Wang et al., 2015), decreasing the stability of the Ag NPs. Even though all Ag NPs suspensions were prepared freshly daily before the measurement, the potential dissolution and higher sedimentation of Ag NPs in DI water may decrease the availability of Ag NPs (Liu and Hurt, 2010; Misra et al., 2012). Simply adding a 1 mM citrate buffer to the suspension resulted in Ag NPs concentrations much closer to the nominal values (Fig. 1A). Citrate buffers or coatings are commonly used to stabilize Ag NPs in suspension (Peters et al., 2014); this should be considered when designing an sp-ICP-MS analysis protocol for higher accuracy. Similar precision was observed in the SWW matrix (Fig. 1B). The presence of organic compounds (e.g., glucose) and other cations (e.g., Na^+, Mg^{2+}, Ca^{2+}) and anions (e.g., Cl^-, SO_4^{2-}, HPO_4^{2-}) within the SWW do not result in significant interference on the detection and quantification of Ag NPs via sp-ICP-MS. sp-ICP-MS also provided a size distribution of Ag NPs in these three water matrixes, as shown in Fig. S4. Generally, the measured sizes by sp-ICP-MS exhibited a peak at around 60 nm (Fig. S4), which agreed with the information provided by the manufacturer. However, the peak of the Ag NP size distribution in DI water was slightly shifted to a smaller range (Fig. S4), indicating some possible dissolution of Ag NPs in DI even in a short time, as inferred from the calibration curve measurements.

3.3. Incidence of Ag NPs in wastewater

The concentrations of Ag NPs and Ag^+ in wastewater samples were quantified using sp-ICP-MS (Fig. 2). Ag NP concentrations were 13.5, 3.2, 0.5 and 9.8 ng/L in the influent, secondary effluent, tertiary reclaimed and backwash water, respectively. These concentrations do not reflect Ag NPs potentially associated with suspended solids, since they would be removed by the nitrocellulose filters (0.45 μm). Silver-based nanomaterials in the WWTP and the environment can include Ag^0, Ag_2O, Ag_2S, and AgCl, which are stable forms of silver (Kaegi et al., 2013; Lowry et al., 2012). To calculate the size distribution of the Ag NPs in the samples, we assumed a 100% silver content and a spherical shape. The size distribution, as determined by sp-ICP-MS, varied significantly at the various stages of treatment. The most frequent particle diameter of

Table 2
Physicochemical characteristics of wastewater samples collected in "El Estero" wastewater treatment plant, influent, effluent, reclaimed water, backwash water, and synthetic wastewater. Average ± Standard deviation. N/A means not applicable.

Parameter	Influent	Effluent	Reclaimed water	Backwash Water	Synthetic Wastewater
pH	7.41 ± 0.13	7.20 ± 0.09	7.23 ± 0.08	7.01 ± 0.11	7.06 ± 0.08
Conductivity (mS/cm)	2.58 ± 0.06	2.22 ± 0.04	2.24 ± 0.08	2.26 ± 0.04	0.18 ± 0.01
Ionic Strength (equiv/L)	0.041 ± 0.001	0.036 ± 0.001	0.036 ± 0.001	0.036 ± 0.001	0.003
Dissolved C (mg/L)	187 ± 4	64 ± 2	37 ± 2	64 ± 4	372 ± 2
TN (mg/L)	197 ± 6	48 ± 1	28 ± 0	55 ± 0	35 ± 2
NH_4^+–N (mg/L)	147 ± 9.1	38.7 ± 0.8	32 ± 0.6	35.4 ± 3.3	19.8 ± 2.9
NO_3–N (mg/L)	4.0 ± 0.2	4.3 ± 0.2	3.2 ± 0.9	3.2 ± 0.2	0.7 ± 0.2
NO_2–N (mg/L)	0.02 ± 0.003	1.2 ± 0.01	0.6 ± 0.01	0.9 ± 0.01	0.01 ± 0.002
PO_4–P (mg/L)	8.8 ± 0.03	2.2 ± 0.02	2.3 ± 0.1	2.3 ± 0.3	4.6 ± 0.3
S^{2-} (mg/L)	3.8 ± 0.5	<0.05	<0.05	<0.05	<0.05
Suspended solids (SS)					
TSS (mg/L)	565 ± 54	120 ± 14	N/A	65 ± 7	N/A
VSS (mg/L)	385 ± 43	100 ± 14	N/A	30 ± 10	N/A
FSS (mg/L)	180 ± 25	20 ± 3	N/A	35 ± 5	N/A

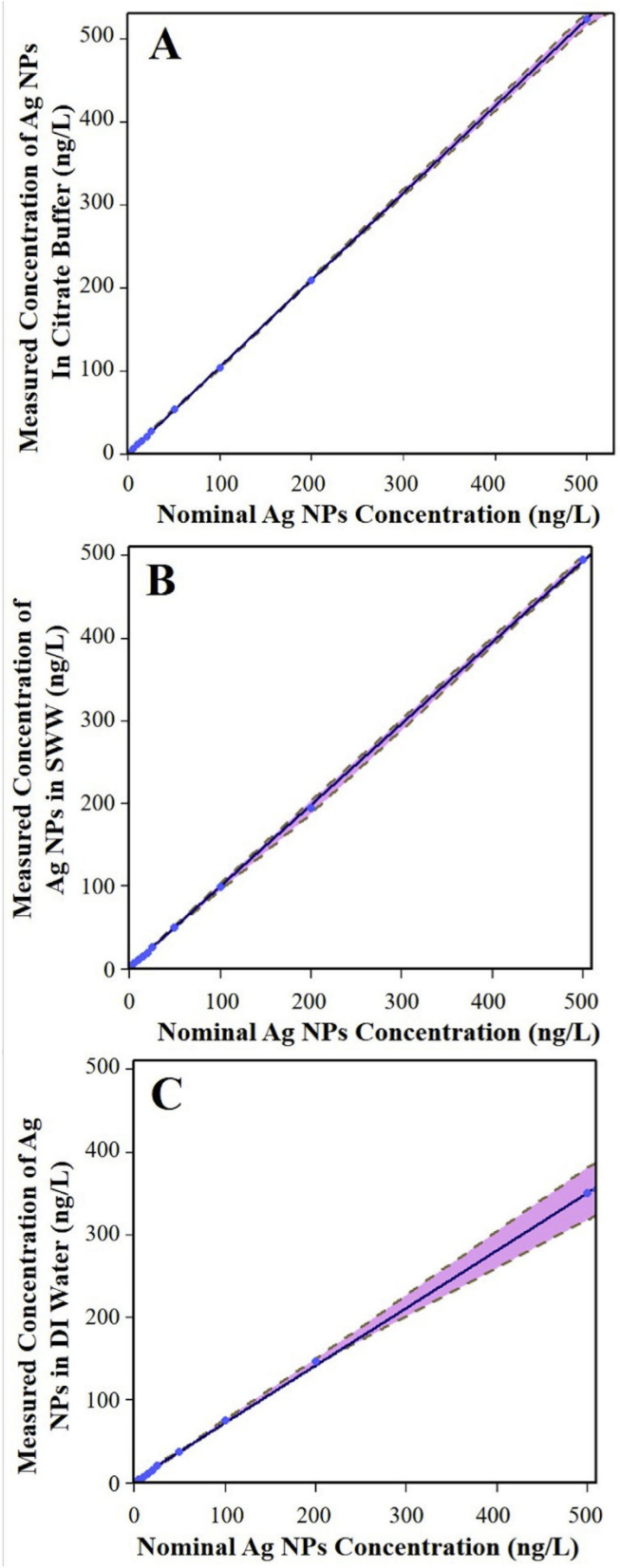

Fig. 1. Calibration curve of Ag NPs concentration in (A) 1 mM citrate buffer solution, (B) synthetic wastewater (SWW) and (C) DI water; blue symbols represent the average of measured values, the blue line represents the linear regression, and the purple shade represents the standard deviations of three replicate measurements. (For interpretation of the references to color in this figure legend, the reader is referred to the Web version of this article.)

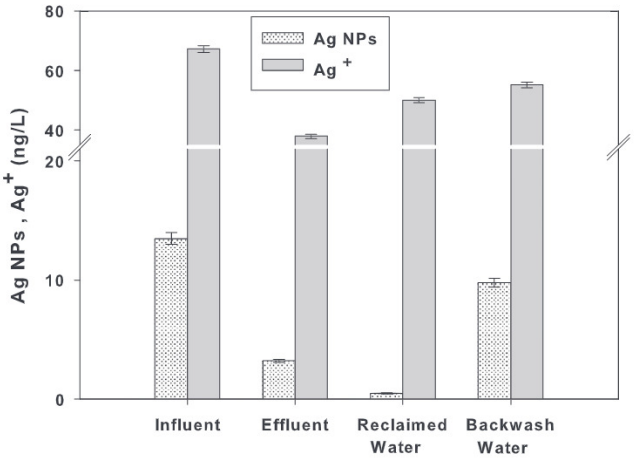

Fig. 2. The concentration of Ag NPs and Ag^+ in samples collected in different points of the wastewater treatment process from El Estero WWTP. Ag NP and Ag^+ values presented relative standard deviations (RSDs) < 5%.

Ag NPs in all types of wastewater was between 20 and 24 nm (Fig. 3); however, the 20 nm cut-off influences the distribution. Ag NPs detected in the influent were mostly below 100 nm in diameter, with a substantial fraction above 50 nm and few particles up to nearly 200 nm. In the effluent most of the Ag NPs were below 50 nm, with very few above 100 nm. After ultrafiltration (100 nm pore size) only NPs between 20 and 45 nm were observed, and at a much lower frequency. The backwash water from the ultrafiltration process did have particles larger than 100 nm, reflecting the difference between the effluent and reclaimed water. The determination of Ag NP particle size by sp-ICP-MS showed a clear limit of detection around 20 nm in diameter. The trend in Fig. 3 strongly suggests that Ag NPs smaller than 20 nm could be present at high numbers in the samples, but this could not be determined with the current analytical protocol (Lee et al., 2014). This limitation has also been observed for other types of NP and aqueous media such as the cases of rare earth oxides in water (Fréchette-Viens et al., 2017); Ag, Au and TiO_2 NPs in drinking water (Donovan et al., 2016) and Ag, CeO_2 and TiO_2 NPs surface water (Peters et al., 2018).

The biological process at El Estero WWTP removed 76.3% of the incidental Ag NPs, and combined with ultrafiltration, the WWTP removed 96.3% of the influent load. In the ultrafiltration system, the particulate matter, including the NPs retained by the membrane, is returned to the influent of the wastewater process. Therefore, 9.8 ng/L of Ag NPs in the backwash water re-enter the biological process, where there can be a significant accumulation depending on the sludge retention time. The presence of Ag NPs in the biological wastewater treatment process can damage the microbial community, and this in turn can impact the treated water quality (Sun et al., 2013). Ag NPs concentrations found in the influent, effluent and reclaimed water of El Estero WWTP (13.5, 3.2 and 0.5 ng/L, respectively) are within the range measured for effluent (1–12 ng/L) of nine WWTPs in Germany determined via extraction by CPE and IER (Li et al., 2013). Compared to techniques based on separation and elemental quantification (Li et al., 2012, 2013), sp-ICP-MS is a simpler and more direct method to determine Ag NPs concentration in wastewater streams. Using sp-ICP-MS, Peters et al. found between 0.3 and 2.5 ng/L of Ag NPs in Dutch surface waters (Peters et al., 2018), where they considered the discharge of municipal wastewater effluent as a possible source of Ag NPs to surface water.

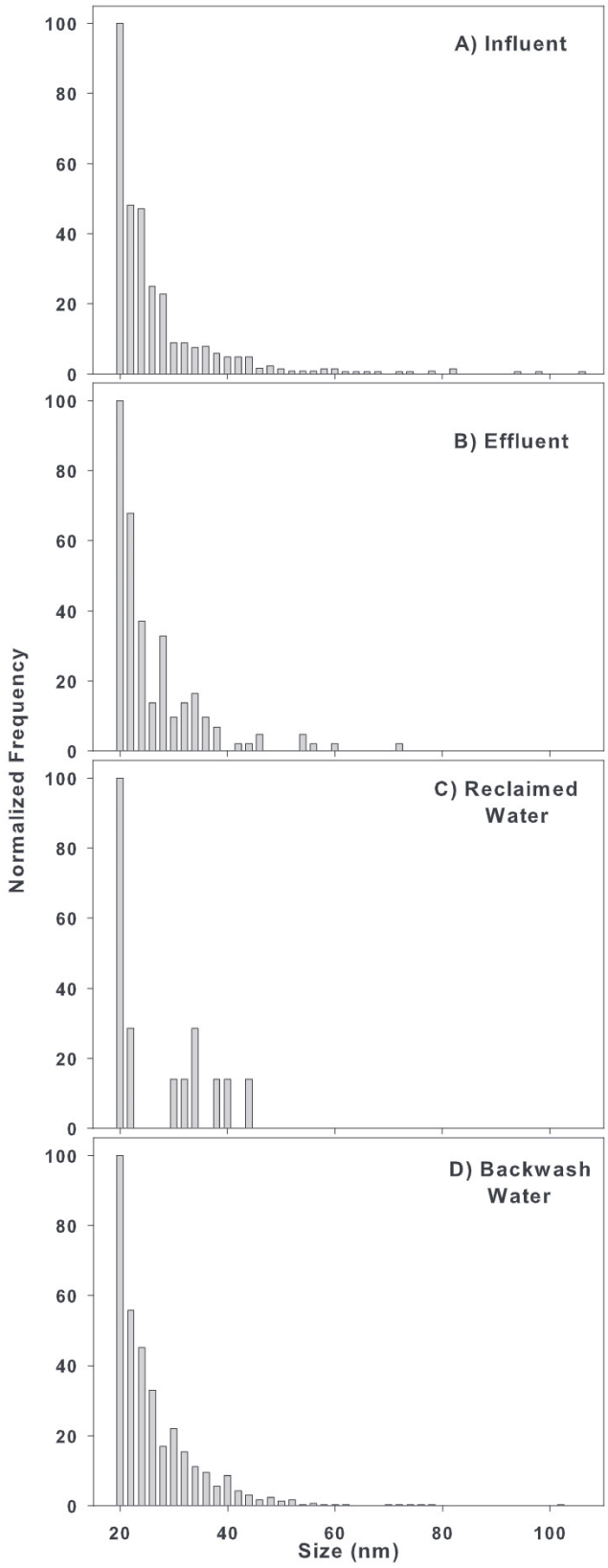

Fig. 3. Size distribution of Ag NPs detected in the wastewater streams in "El Estero" WWTP: A) Influent, B) Effluent, C) Reclaimed water and D) Backwash water.

Ionic concentrations of silver (Ag^+) were 62.2, 37.9, 50.1 and 55.2 ng/L in the influent, effluent, reclaimed and backwash water, respectively. The ratio of Ag^+ to Ag NPs observed in the influent was 4.99, and it increased as the treatment progressed (Fig. 2). The potential accumulation of Ag NPs in the flocs of activated sludge can explain the increase in the ratio. Then, Ag NP can dissolve during the 8 h hydraulic retention time, which is the typical period in the aerobic reactor of a WWTP (Metcalf and Eddy, 2014). The coexistence of Ag^+ and Ag NPs had a negligible effect on the determination of the Ag NP concentrations using sp-ICP-MS in simpler aqueous media (Laborda et al., 2011). Although in our study the various wastewater matrices are complex, we did not observe a noticeable effect due to the coexistence of Ag^+ and Ag NPs. In contrast, high Ag^+ content significantly interferes with Ag NP quantification using IER followed by Analytical Graphite Furnace Atomic Absorption Spectrometry (GFAAS) (Li et al., 2013). The interference was attributed to simultaneous extraction of Ag^+ and Ag NP, which can be falsely quantified as Ag NP by the GFAAS analysis.

Several studies have predicted the range of Ag NP and released Ag^+ concentrations present in the effluent of WWTPs or receiving waters at different geographic scales, from cities to continental regions. For WWTP effluent in cities the range is 9–120 ng/L in the San Francisco Bay (Keller and Lazareva, 2013), and 4–26 ng/L, 8–130 ng/L and 3–110 ng/L in New York, Shanghai, and London, respectively (Lazareva and Keller, 2014). For the US the range is 1.1–240 ng/L (Hendren et al., 2013), and for Europe the predicted range is 50–100 ng/L (Gottschalk et al., 2013). The concentration of Ag NPs found in effluent at El Estero WWTP is closer to the lower bound of predicted concentrations, and when Ag^+ is taken into consideration there is a very good correspondence with the predicted range. These concentrations were measured in the water column only, and represent the colloidal and ionic silver fractions in the various steps of the wastewater treatment processes, but may not account for silver in larger particles which were removed by the 0.45 μm nitrocellulose filter. Given the high removal from influent to secondary and tertiary effluents observed here, the majority of Ag NPs are in the sludge (Polesel et al., 2018; Tuoriniemi et al., 2017).

3.4. Persistence of Ag NPs in the water column

Ag NPs are well known to dissolve and aggregate in suspension. Knowing how long they can persist in various waters is important for understanding their risk. To study the persistence of Ag NPs in various wastewaters, 300 ng/L of Ag NPs (40 nm) were spiked in influent, effluent, reclaimed water and SWW samples. All wastewater matrixes were filtered with 0.45 μm nitrocellulose filter papers before being spiked with Ag NPs. The Ag NPs and Ag^+ concentration before and after spiking were measured over time. The total Ag concentration at time 0 h for all wastewater matrixes includes the 300 ng/L spiked and the background concentration (pre-spiking) for each water matrix (Fig. 4). Ag^+ remarkably increased in real wastewater matrixes at time 0 h, indicating rapid dissolution of a fraction of the spiked Ag NPs in these waters. Over the monitoring time, the concentration of Ag NP exhibited a remarkable decrease, especially in SWW and influent. The pattern for the influent water was quite predictable, with a regular decrease over time, for both Ag NPs and Ag^+. Since SWW and the influent have a greater amount of organic matter, nitrogen, phosphorus, chlorine, and sulfur, the decrease of free Ag^+ in wastewater could be due to the formation of organic complexes (Zhang et al., 2016a), or inorganic salts with low solubility such as AgCl and Ag_2S (Kaegi et al., 2013; Lombi et al., 2013). In contrast, the concentrations of Ag NPs and Ag^+ in secondary effluent and tertiary reclaimed water

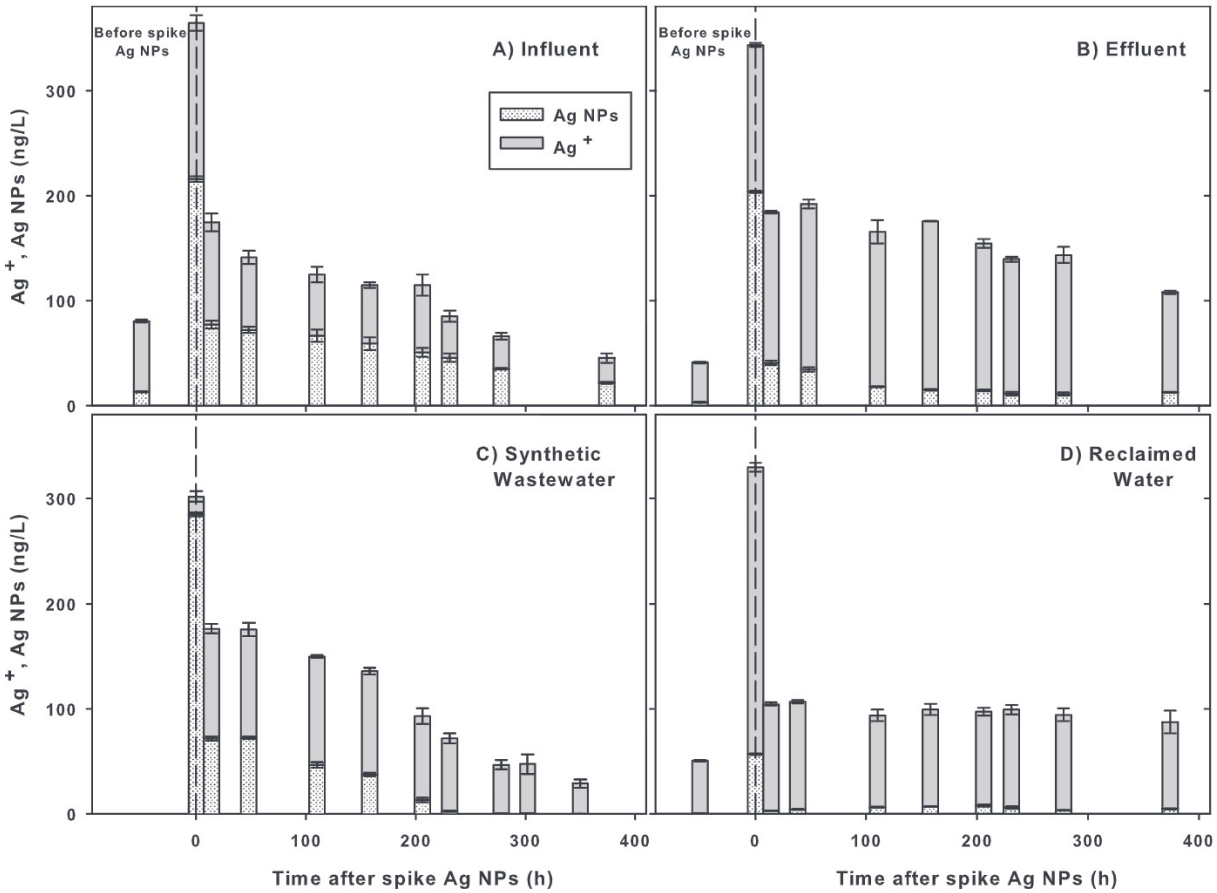

Fig. 4. The concentration of Ag NPs and Ag^{+} before and after spike 300 ng/L of Ag NPs (40 nm) in wastewater streams: A) Influent, B) Effluent, C) Synthetic wastewater and D) Reclaimed water.

remained relatively constant between 14 h and 300 h (Fig. 4). After 374 h, there was a significant amount of precipitate in all wastewater samples. The results indicate that the persistence in suspension of Ag NPs followed influent > secondary effluent > tertiary reclaimed > SWW.

The size distribution of the Ag NPs over time (0–374 h) was also determined by sp-ICP-MS and represented in violin plots (Fig. 5). The shape of each violin plot represents the frequency of Ag NPs size that occurs 95% of the time (blue region), and the inner box represents the sizes that occur 50% of the time. The central dash line inside the white box represents the median value of the Ag NPs size. Based on the median size (dash line), the results indicate that only Ag NPs in the influent maintained their original (nominal) size distribution during the entire study time, which was 42 ± 5 nm (Fig. 5A). Ag NPs in SWW had a median size of 39 ± 4 nm (Fig. 5C) which remained relatively constant for the entire monitored time. However, after 206 h the detection of Ag NPs in SWW was limited to a few counts (Fig. 4), indicating significant settling, and resulting in distorted plots at 231 and 278 h. In secondary effluent the size distribution of Ag NPs varied with time, with the median value oscillating from 40 to 43 nm (Fig. 5B). Despite the variations of the median, the frequency of Ag NPs size that occurs 95% of the time in the effluent showed a peak (blue region) around 36 nm in all measurements. Although the Ag NPs concentrations measured in reclaimed water along the experiment were the lowest (Fig. 4), the size distribution had the same pattern at 374 h (Fig. 5D), with higher frequency in the size range of 34–36 nm. The analysis of Ag NP size occurring 95% of the time confirms that most of the dissolution of Ag NPs happened before 14 h in the effluent and reclaimed water, based on the decrease in nominal Ag NP size.

The size distribution of Ag NPs in various waters at 14 h and 374 h are presented in the supplementary material (Fig. S5). Analysis of Ag NP size in all wastewater matrices indicates that the frequency of particles larger than 50 nm decreased between 14 h and 374 h of retention time (Fig. S5). In the case of the influent, only 3.3% of the particles were >100 nm at 14 h, and at 374 h there were no particles >100 nm. The relatively constant size of Ag NPs in the influent can be attributed to the organic matter content present, which stabilizes NP suspensions by the physical and chemical interactions mentioned before (Kaegi et al., 2013; Wang et al., 2015). For the effluent 85.8% of the particles were below 50 nm at 374 h of exposure. The fraction of larger particles in reclaimed water also decreased at 374 h, with 88.2% of the particles smaller than 50 nm, and 11.8% between 50 and 100 nm. Results indicate that the spiked Ag NPs (40 nm) in contact with the outlet streams of the WWTP (effluent and reclaimed water) are mainly dissolved, and between 85 and 89% of the remaining Ag NPs are below 50 nm.

The bottles containing the Ag NPs were vortexed at the end of the experiment to determine the recovery of Ag NPs relative to the mass spiked in, as well as the Ag^{+} concentration (Fig. 6). Consideration of the Ag particulate and ionic concentrations can serve to determine the extent of dissolution and precipitation. The recovered concentration of Ag NPs spiked in SWW was higher (92.72 ng/L), than in the other types of wastewater, such as influent (51.34 ng/L), effluent (23.98 ng/L) and reclaimed (8.17 ng/L). While Ag NPs were almost totally dissolved in reclaimed water (97.28%), in SWW only 69.09% were dissolved, with the balanced in the colloidal fraction (30.91%). Given that there were no colloidal particles in

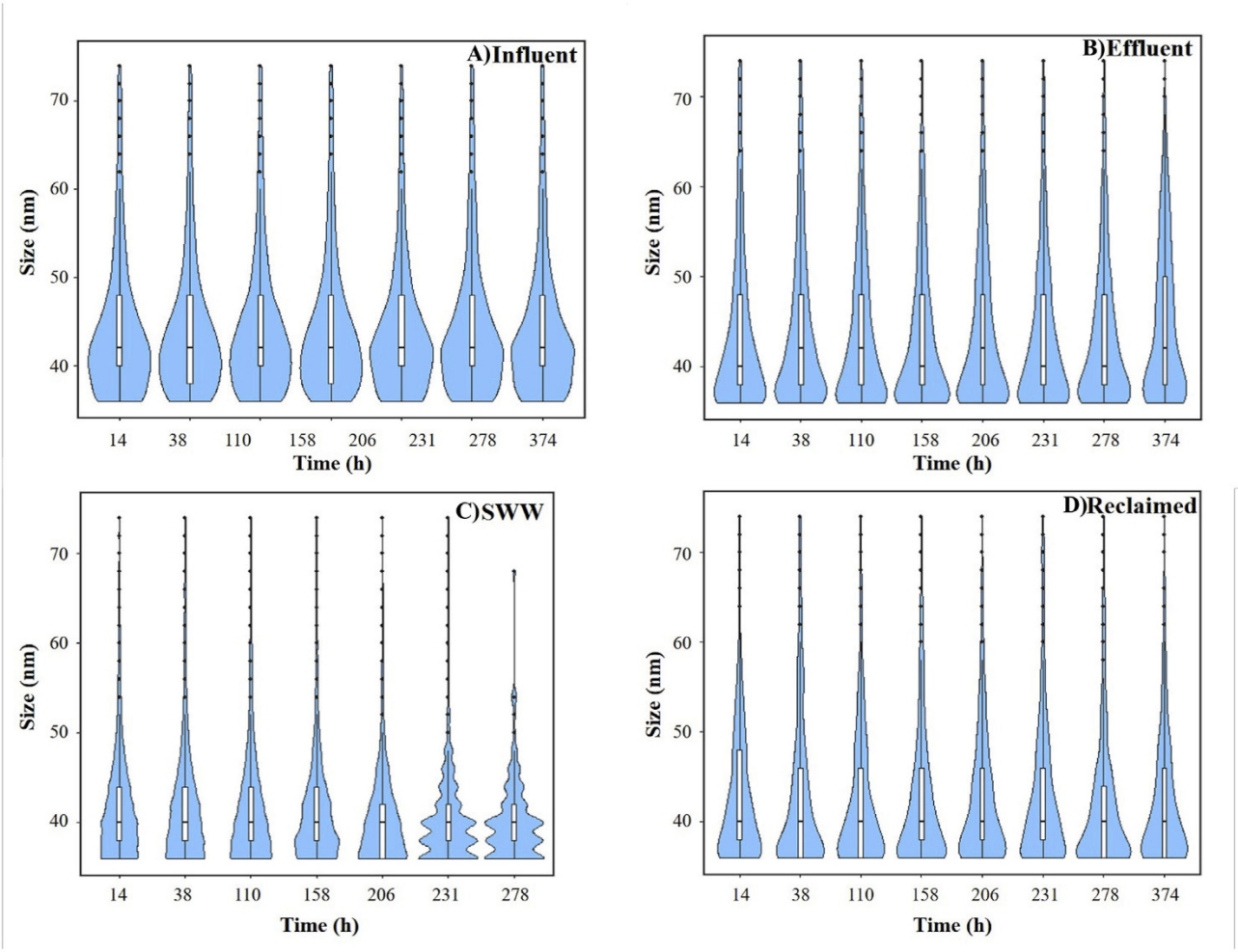

Fig. 5. Violin plots of the size distribution of Ag NPs during 374 h of monitoring after spiking 300 ng/L of Ag NPs (40 nm) in: A) Influent, B) Effluent, C) Synthetic wastewater and D) Reclaimed water. Note: The shape of each violin plot represents the sizes of Ag NPs that occur 95% of the time, and the inner box represents the values that occur 50% of the time. The central dash line represents the median value of the Ag NPs size.

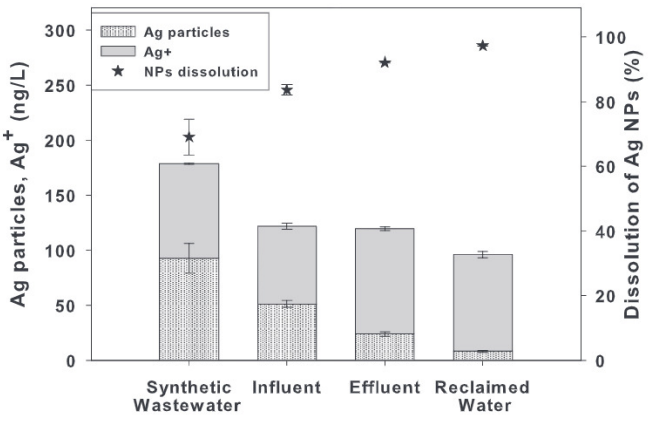

Fig. 6. The recovered concentration of Ag NPs and Ag^{+}, and dissolution percent after spiking 300 ng/L and left to stand for 15 days in different wastewater streams: Synthetic wastewater, influent, effluent, and reclaimed water.

SWW at 204 h (Fig. 4), the balance was indeed precipitated. Ag ionic concentration in wastewater samples were 85.8, 70.4, 95.5 and 87.9 ng/L for SWW, influent, effluent and reclaimed water. These values reflect that a fraction of initial Ag NPs precipitated as transformation products non-detectable in suspension.

The stability of Ag NPs in various wastewaters was studied further by determining the IEP and ZP of the particles immediately after spiking and at 374 h. The ZP of the Ag NPs decreased during the study period for SWW, influent and effluent (Fig. S6), although the change was more significant for SWW. The opposite behavior was found for Ag NPs in reclaimed water, where the ZP increased slightly. Minor changes in ZP were observed for effluent and reclaimed water, which is consistent with the persistence of Ag NPs in suspension at 374 h.

The IEP of the spiked Ag NPs was between pH 2 and 3 in all wastewaters (Fig. S7), which means the Ag NPs are negatively charged in the typical range of WWTP operating conditions. The IEP provides valuable information about the layer composition on the particle surface, such as the acid or basic surface functional groups. The IEP curves for influent, effluent, reclaimed water and SWW suggest that the Ag NPs have anionic compounds on the surface (Fig. S7). The constant negative charge on the surface of the particles in the range of pH 4–10 suggests that those compounds present in the wastewater streams are tightly bound. The ZP in the influent and in the reclaimed water remained between −13 and −15 mV for the typical pH range of 5–9 in wastewater (van Loosdrecht et al., 2016), while the ZP in the effluent was near −10

mV. For SWW, the ZP was more negative as pH increased, enhancing the stability of Ag NPs. Hence, the settling of Ag NPs in SWW was due to the rapid initial formation of larger aggregates (Fig. S5), and not due to the decreasing ZP of the NPs remaining in suspension (Fig. S6). Aggregates formation can be attributed to the presence of cations such as Ca^{2+} and Mg^{2+} (Hotze et al., 2010), which are components of the SWW.

4. Conclusions

sp-ICP-MS was applied to determine the concentration (number and mass) and size of Ag NPs in different water matrixes, as well as to investigate the incidence and persistence of Ag NPs in wastewater through the treatment process. Ag NPs were detected and quantified in influent, secondary effluent, tertiary reclaimed and backwash waters with a concentration of 13.5, 3.2, 0.5 and 9.8 ng/L, respectively, which correspond well with previously predicted wastewater effluent concentrations. A conventional WWTP process followed by ultrafiltration removed more than 96% of the colloidal silver fraction. However, since the UF backwash water is returned to the secondary treatment, the accumulation of NPs in the activated sludge increases both the concentration in a bioreactor and their residence time in the process, which may eventually affect the biological process. Most of the incidental Ag NPs detected in the influent were below 100 nm in diameter, although some NPs were nearly 200 nm. In the effluent, almost all particles were below 50 nm with few above 100 nm. Reclaimed water contained particles between 20 and 45 nm and backwash water had the larger particles, retained by the UF membrane. The persistence in suspension of Ag NPs in wastewater streams revealed that although Ag NPs dissolved in wastewater, the remaining NPs tended to precipitate due to their lower stability in SWW, influent and effluent, respectively. The persistence in suspension of Ag NPs followed influent > effluent > reclaimed > SWW. Dissolution of Ag NPs was observed in all WWTP waters mainly at time 0 h. Spiked Ag NPs remain near their original size in the influent and in the SWW. For effluent and reclaimed water, 95% of the NPs were between 34 and 36 nm. Although the measured concentrations in the wastewater flows in the WWTP, influent, effluent and reclaimed waters, were very low (13.5, 3.2 and 0.5 ng/L, respectively) and only reflect the colloidal fractions in the effluents; the sampling regime performed may mask the actual variability in the Ag NP concentration.

Acknowledgments

This work was supported by the National Science Foundation (NSF) and the U.S. Environmental Protection Agency (EPA) under cooperative agreement number NSF-EF0830117. Arturo A. Keller also appreciates Agilent Technologies for their Agilent Thought Leader Award. Pabel Cervantes-Aviles thanks CONACYT for his postdoctoral fellowship (330129). The authors thank Dr. Yuwei Qin for her help with data analysis. Any opinions, findings, conclusions, or recommendations expressed in this material are those of the authors do not necessarily reflect the views of the funding agencies.

Appendix A. Supplementary data

Supplementary data to this article can be found online at https://doi.org/10.1016/j.watres.2019.03.031.

References

APHA, 2005. Standard methods for the examination of water and wastewater. Stand. Methods 541. https://doi.org/ISBN 9780875532356.

Azimzada, A., Tufenkji, N., Wilkinson, K.J., 2017. Transformations of silver nanoparticles in wastewater effluents: links to Ag bioavailability. Environ. Sci. Nano 4, 1339–1349. https://doi.org/10.1039/c7en00093f.

Aznar, R., Barahona, F., Geiss, O., Ponti, J., José Luis, T., Barrero-Moreno, J., 2017. Quantification and size characterisation of silver nanoparticles in environmental aqueous samples and consumer products by single particle-ICPMS. Talanta 175, 200–208. https://doi.org/10.1016/j.talanta.2017.07.048.

Blaser, S.A., Scheringer, M., MacLeod, M., Hungerbühler, K., 2008. Estimation of cumulative aquatic exposure and risk due to silver: contribution of nano-functionalized plastics and textiles. Sci. Total Environ. 390, 396–409. https://doi.org/10.1016/j.scitotenv.2007.10.010.

Cao, C., Huang, J., Yan, C., Liu, J., Hu, Q., Guan, W., 2018. Shifts of system performance and microbial community structure in a constructed wetland after exposing silver nanoparticles. Chemosphere 199, e34. https://doi.org/10.1016/j.chemosphere.2018.02.031.

Cascio, C., Geiss, O., Franchini, F., Ojea-Jimenez, I., Rossi, F., Gilliland, D., Calzolai, L., 2015. Detection, quantification and derivation of number size distribution of silver nanoparticles in antimicrobial consumer products. J. Anal. At. Spectrom. 30, 1255–1265. https://doi.org/10.1039/c4ja00410h.

Cervantes-Avilés, P., Díaz Barriga-Castro, E., Palma-Tirado, L., Cuevas-Rodríguez, G., 2017. Interactions and effects of metal oxide nanoparticles on microorganisms involved in biological wastewater treatment. Microsc. Res. Tech. 80, 1103–1112. https://doi.org/10.1002/jemt.22907.

Chan, C., Guisasola, A., Baeza, J.A., 2017. Enhanced biological phosphorus removal at low sludge retention time in view of its integration in A-stage systems. Water Res. 118, 217–226. https://doi.org/10.1016/j.watres.2017.04.010.

Chao, J., Liu, J., Yu, S., Feng, Y., Tan, Z., Liu, R., Yin, Y., 2011. Speciation analysis of silver nanoparticles and silver ions in antibacterial products and environmental waters via cloud point extraction-based separation. Anal. Chem. 83, 6875–6882. https://doi.org/10.1021/ac201086a.

Chinnapongse, S.L., MacCuspie, R.I., Hackley, V.A., 2011. Persistence of singly dispersed silver nanoparticles in natural freshwaters, synthetic seawater, and simulated estuarine waters. Sci. Total Environ. 409, 2443–2450. https://doi.org/https://doi.org/10.1016/j.scitotenv.2011.03.020.

Choi, O., Hu, Z., 2008. Size dependent and reactive oxygen species related nanosilver toxicity to nitrifying bacteria. Environ. Sci. Technol. 42, 4583–4588. https://doi.org/10.1021/es703238h.

Choi, S., Johnston, M.V., Wang, G.S., Huang, C.P., 2017. Looking for engineered nanoparticles (ENPs) in wastewater treatment systems: qualification and quantification aspects. Sci. Total Environ. 590–591, 809–817. https://doi.org/10.1016/j.scitotenv.2017.03.061.

Cuevas-Rodríguez, G., Cervantes-Avilés, P., Torres-Chávez, I., Bernal-Martínez, A., 2015. Evaluation of different configurations of hybrid membrane bioreactors for treatment of domestic wastewater. Water Sci. Technol. 71, 338–346. https://doi.org/10.2166/wst.2014.481.

de la Calle, I., Menta, M., Klein, M., Séby, F., 2017. Screening of TiO2 and Au nanoparticles in cosmetics and determination of elemental impurities by multiple techniques (DLS, SP-ICP-MS, ICP-MS and ICP-OES). Talanta 171, 291–306. https://doi.org/10.1016/j.talanta.2017.05.002.

Donovan, A.R., Adams, C.D., Ma, Y., Stephan, C., Eichholz, T., Shi, H., 2016. Single particle ICP-MS characterization of titanium dioxide, silver, and gold nanoparticles during drinking water treatment. Chemosphere 144, 148–153. https://doi.org/10.1016/j.chemosphere.2015.07.081.

Doolette, C.L., McLaughlin, M.J., Kirby, J.K., Batstone, D.J., Harris, H.H., Ge, H., Cornelis, G., 2013. Transformation of PVP coated silver nanoparticles in a simulated wastewater treatment process and the effect on microbial communities. Chem. Cent. J. 7, 1. https://doi.org/10.1186/1752-153X-7-46.

Echavarri-Bravo, V., Paterson, L., Aspray, T.J., Porter, J.S., Winson, M.K., Hartl, M.G.J., 2017. Natural marine bacteria as model organisms for the hazard-assessment of consumer products containing silver nanoparticles. Mar. Environ. Res. 130, 293–302. https://doi.org/10.1016/j.marenvres.2017.08.006.

Fréchette-Viens, L., Hadioui, M., Wilkinson, K.J., 2017. Practical limitations of single particle ICP-MS in the determination of nanoparticle size distributions and dissolution: case of rare earth oxides. Talanta 163, 121–126. https://doi.org/10.1016/j.talanta.2016.10.093.

Gartiser, S., Flach, F., Nickel, C., Stintz, M., Damme, S., Schaeffer, A., Erdinger, L., Kuhlbusch, T.A.J., 2014. Behavior of nanoscale titanium dioxide in laboratory wastewater treatment plants according to OECD 303 A. Chemosphere 104, 197–204. https://doi.org/10.1016/j.chemosphere.2013.11.015.

Gottschalk, F., Sun, T., Nowack, B., 2013. Environmental concentrations of engineered nanomaterials: review of modeling and analytical studies. Environ. Pollut. 181, 287–300. https://doi.org/10.1016/j.envpol.2013.06.003.

Guo, H., Xing, B., Hamlet, L.C., Chica, A., He, L., 2016. Surface-enhanced Raman scattering detection of silver nanoparticles in environmental and biological samples. Sci. Total Environ. 554 (555), 246–252. https://doi.org/10.1016/j.scitotenv.2016.02.084.

Hadioui, M., Peyrot, C., Wilkinson, K.J., 2014. Improvements to single particle ICPMS by the online coupling of ion exchange resins. Anal. Chem. 86, 4668–4674. https://doi.org/10.1021/ac5004932.

Hendren, C.O., Badireddy, A.R., Casman, E., Wiesner, M.R., 2013. Modeling nanomaterial fate in wastewater treatment: Monte Carlo simulation of silver nanoparticles (nano-Ag). Sci. Total Environ. 449, 418–425. https://doi.org/10.1016/j.scitotenv.2013.01.078.

Holden, P.A., Gardea-Torresdey, J.L., Klaessig, F., Turco, R.F., Mortimer, M., Hund-Rinke, K., Cohen Hubal, E.A., Avery, D., Barceló, D., Behra, R., Cohen, Y., Deydier-Stephan, L., Ferguson, P.L., Fernandes, T.F., Herr Harthorn, B., Henderson, W.M.,

Hoke, R.A., Hristozov, D., Johnston, J.M., Kane, A.B., Kapustka, L., Keller, A.A., Lenihan, H.S., Lovell, W., Murphy, C.J., Nisbet, R.M., Petersen, E.J., Salinas, E.R., Scheringer, M., Sharma, M., Speed, D.E., Sultan, Y., Westerhoff, P., White, J.C., Wiesner, M.R., Wong, E.M., Xing, B., Steele Horan, M., Godwin, H.A., Nel, A.E., 2016. Considerations of environmentally relevant test conditions for improved evaluation of ecological hazards of engineered nanomaterials. Environ. Sci. Technol. 50.

Hotze, E.M., Phenrat, T., Lowry, G.V., 2010. Nanoparticle aggregation: challenges to understanding transport and reactivity in the environment. J. Environ. Qual. 39, 1909. https://doi.org/10.2134/jeq2009.0462.

Hou, L., Li, K., Ding, Y., Li, Y., Chen, J., Wu, X., Li, X., 2012. Removal of silver nanoparticles in simulated wastewater treatment processes and its impact on COD and NH4reduction. Chemosphere 87, 248–252. https://doi.org/10.1016/j.chemosphere.2011.12.042.

Impellitteri, C.A., Tolaymat, T.M., Scheckel, K.G., 2009. The speciation of silver nanoparticles in antimicrobial fabric before and after exposure to a hypochlorite/detergent solution. J. Environ. Qual. 38, 1528. https://doi.org/10.2134/jeq2008.0390.

Ivask, A., Kurvet, I., Kasemets, K., Blinova, I., Aruoja, V., Suppi, S., Vija, H., Kakinen, A., Titma, T., Heinlaan, M., Visnapuu, M., Koller, D., Kisand, V., Kahru, A., 2014. Size-dependent toxicity of silver nanoparticles to bacteria, yeast, algae, crustaceans and mammalian cells in vitro. PLoS One 9. https://doi.org/10.1371/journal.pone.0102108.

Kaegi, R., Voegelin, A., Ort, C., Sinnet, B., Thalmann, B., Krismer, J., Hagendorfer, H., Elumelu, M., Mueller, E., 2013. Fate and transformation of silver nanoparticles in urban wastewater systems. Water Res. 47, 3866–3877. https://doi.org/10.1016/j.watres.2012.11.060.

Kaegi, R., Voegelin, A., Sinnet, B., Zuleeg, S., Hagendorfer, H., Burkhardt, M., Siegrist, H., 2011. Behavior of metallic silver nanoparticles in a pilot wastewater treatment plant. Environ. Sci. Technol. 45, 3902–3908. https://doi.org/10.1021/es1041892.

Keller, A.A., Huang, Y., Nelson, J., 2018. Detection of nanoparticles in edible plant tissues exposed to nano-copper using single-particle ICP-MS. J. Nanoparticle Res. 20. https://doi.org/10.1007/s11051-018-4192-8.

Keller, A.A., Lazareva, A., 2013. Predicted releases of engineered nanomaterials: from global to regional to local. Environ. Sci. Technol. Lett. 1, 65–70. https://doi.org/10.1021/ez400106t.

Laborda, F., Bolea, E., Cepriá, G., Gómez, M.T., Jiménez, M.S., Pérez-Arantegui, J., Castillo, J.R., 2016. Detection, characterization and quantification of inorganic engineered nanomaterials: a review of techniques and methodological approaches for the analysis of complex samples. Anal. Chim. Acta 904, 10–32. https://doi.org/10.1016/j.aca.2015.11.008.

Laborda, F., Bolea, E., Jiménez-Lamana, J., 2014. Single particle inductively coupled plasma mass spectrometry: a powerful tool for nanoanalysis. Anal. Chem. 86, 2270–2278. https://doi.org/10.1021/ac402980q.

Laborda, F., Jiménez-Lamana, J., Bolea, E., Castillo, J.R., 2011. Selective identification, characterization and determination of dissolved silver(i) and silver nanoparticles based on single particle detection by inductively coupled plasma mass spectrometry. J. Anal. At. Spectrom. 26, 1362–1371. https://doi.org/10.1039/C0JA00098A.

Lalley, J., Dionysiou, D.D., Varma, R.S., Shankara, S., Yang, D.J., Nadagouda, M.N., 2014. Silver-based antibacterial surfaces for drinking water disinfection - an overview. Curr. Opin. Chem. Eng. 3, 25–29. https://doi.org/10.1016/j.coche.2013.09.004.

Lazareva, A., Keller, A.A., 2014. Estimating potential life cycle releases of engineered nanomaterials from wastewater treatment plants. ACS Sustain. Chem. Eng. 2, 1656–1665. https://doi.org/10.1021/sc500121w.

Lee, S., Bi, X., Reed, R.B., Ranville, J.F., Herckes, P., Westerhoff, P., 2014. Nanoparticle size detection limits by single particle ICP-MS for 40 elements. Environ. Sci. Technol. 48, 10291–10300. https://doi.org/10.1021/es502422v.

Levard, C., Hotze, E.M., Colman, B.P., Dale, A.L., Truong, L., Yang, X.Y., Bone, A.J., Brown, G.E., Tanguay, R.L., Di Giulio, R.T., Bernhardt, E.S., Meyer, J.N., Wiesner, M.R., Lowry, G.V., 2013a. Sulfidation of silver nanoparticles: natural antidote to their toxicity. Environ. Sci. Technol. 47, 13440–13448. https://doi.org/10.1021/es403527n.

Levard, C., Mitra, S., Yang, T., Jew, A.D., Badireddy, A.R., Lowry, G.V., Brown, G.E., 2013b. Effect of chloride on the dissolution rate of silver nanoparticles and toxicity to E. coli. Environ. Sci. Technol. 47, 5738–5745. https://doi.org/10.1021/es400396f.

Li, L., Hartmann, G., Döblinger, M., Schuster, M., 2013. Quantification of nanoscale silver particles removal and release from municipal wastewater treatment plants in Germany. Environ. Sci. Technol. 47, 7317–7323. https://doi.org/10.1021/es3041658.

Li, L., Leopold, K., Schuster, M., 2012. Effective and selective extraction of noble metal nanoparticles from environmental water through a noncovalent reversible reaction on an ionic exchange resin. Chem. Commun. 48, 9165–9167. https://doi.org/10.1039/c2cc34838a.

Liu, J., Hurt, R.H., 2010. Ion release kinetics and particle persistence in aqueous nano-silver colloids. Environ. Sci. Technol. 44, 2169–2175. https://doi.org/10.1021/es9035557.

Liu, Y., Tourbin, M., Lachaize, S., Guiraud, P., 2014. Nanoparticles in wastewaters: hazards, fate and remediation. Powder Technol. 255, 149–156. https://doi.org/10.1016/j.powtec.2013.08.025.

Lombi, E., Donner, E., Taheri, S., Tavakkoli, E., Jamting, Å.K., McClure, S., Naidu, R., Miller, B.W., Scheckel, K.G., Vasilev, K., 2013. Transformation of four silver/silver chloride nanoparticles during anaerobic treatment of wastewater and post-processing of sewage sludge. Environ. Pollut. 176, 193–197.

Lowry, G.V., Espinasse, B.P., Badireddy, A.R., Richardson, C.J., Reinsch, B.C., Bryant, L.D., Bone, A.J., Deonarine, A., Chae, S., Therezien, M., Colman, B.P., Hsu-Kim, H., Bernhardt, E.S., Matson, C.W., Wiesner, M.R., 2012. Long-term transformation and fate of manufactured Ag nanoparticles in a simulated large scale freshwater emergent wetland. Environ. Sci. Technol. 46, 7027–7036. https://doi.org/10.1021/es204608d.

Ma, R., Levard, C., Judy, J.D., Unrine, J.M., Durenkamp, M., Martin, B., Jefferson, B., Lowry, G.V., 2013a. Fate of zinc oxide and silver nanoparticles in a pilot wastewater treatment plant and in processed biosolids. Environ. Sci. Technol. 48, 104–112. https://doi.org/10.1021/es403646x.

Ma, R., Levard, C., Judy, J.D., Unrine, J.M., Martin, B., Jefferson, B., Lowry, G.V., Durenkamp, M., 2013b. Fate of Zinc Oxide and Silver Nanoparticles in a Pilot Waste Water Treatment Plant and in Processed Biosolids Fate of Zinc Oxide and Silver Nanoparticles in a Pilot Waste Water Treatment Plant and in Processed Biosolids.

Maurer-Jones, M.A., Gunsolus, I.L., Murphy, C.J., Haynes, C.L., 2013. Toxicity of engineered nanoparticles in the environment. Anal. Chem. 85, 3036–3049. https://doi.org/10.1021/ac303636s.

McGillicuddy, E., Murray, I., Kavanagh, S., Morrison, L., Fogarty, A., Cormican, M., Dockery, P., Prendergast, M., Rowan, N., Morris, D., 2017. Silver nanoparticles in the environment: sources, detection and ecotoxicology. Sci. Total Environ. 575, 231–246. https://doi.org/10.1016/j.scitotenv.2016.10.041.

Metcalf, E., Eddy, M., 2014. Wastewater Engineering: Treatment and Resource Recovery. Mic Graw-Hill, USA, pp. 1530–1533.

Misra, S.K., Dybowska, A., Berhanu, D., Luoma, S.N., Valsami-jones, E., 2012. Science of the Total Environment the complexity of nanoparticle dissolution and its importance in nanotoxicological studies. Sci. Total Environ. 438, 225–232. https://doi.org/10.1016/j.scitotenv.2012.08.066.

Mitrano, D.M., Lesher, E.K., Bednar, A., Monserud, J., Higgins, C.P., Ranville, J.F., 2012. Detecting nanoparticulate silver using single-particle inductively coupled plasma-mass spectrometry. Environ. Toxicol. Chem. 31, 115–121. https://doi.org/10.1002/etc.719.

Montaño, M.D., Badiei, H.R., Bazargan, S., Ranville, J.F., 2014. Improvements in the detection and characterization of engineered nanoparticles using spICP-MS with microsecond dwell times. Environ. Sci. Nano 1, 338–346. https://doi.org/10.1039/c4en00058g.

Musee, N., 2017. A model for screening and prioritizing consumer nanoproduct risks: a case study from South Africa. Environ. Int. 100, 121–131. https://doi.org/10.1016/j.envint.2017.01.002.

Nielsen, S.S., 2010. Phenol-sulfuric acid method for total carbohydrates. In: Nielsen, S.S. (Ed.), Food Analysis Laboratory Manual. Springer US, Boston, MA, pp. 47–53. https://doi.org/10.1007/978-1-4419-1463-7_6.

Park, H.J., Kim, H.Y., Cha, S., Ahn, C.H., Roh, J., Park, S., Kim, S., Choi, K., Yi, J., Kim, Y., Yoon, J., 2013. Removal characteristics of engineered nanoparticles by activated sludge. Chemosphere 92, 524–528. https://doi.org/10.1016/j.chemosphere.2013.03.020.

Peters, R.J.B., Rivera, Z.H., van Bemmel, G., Marvin, H.J.P., Weigel, S., Bouwmeester, H., 2014. Development and validation of single particle ICP-MS for sizing and quantitative determination of nano-silver in chicken meat. Anal. Bioanal. Chem. 406, 3875–3885. https://doi.org/10.1007/s00216-013-7571-0.

Peters, R.J.B., van Bemmel, G., Milani, N.B.L., den Hertog, G.C.T., Undas, A.K., van der Lee, M., Bouwmeester, H., 2018. Detection of nanoparticles in Dutch surface waters. Sci. Total Environ. 621, 210–218. https://doi.org/10.1016/j.scitotenv.2017.11.238.

Polesel, F., Farkas, J., Kjos, M., Almeida Carvalho, P., Flores-Alsina, X., Gernaey, K.V., Hansen, S.F., Plósz, B.G., Booth, A.M., 2018. Occurrence, characterisation and fate of (nano)particulate Ti and Ag in two Norwegian wastewater treatment plants. Water Res. 141, 19–31. https://doi.org/10.1016/j.watres.2018.04.065.

Ponnamperuma, F.N., Tianco, E.M., Loy, T.A., 1966. Ionic strengths of the solutions of flooded soils and other natural aqueous solutions from specific conductance. Soil Sci. 102.

Shen, W., Zhang, X., Huang, Q., Xu, Q., Song, W., 2014. Preparation of solid silver nanoparticles for inkjet printed flexible electronics with high conductivity. Nanoscale 6, 1622–1628. https://doi.org/10.1039/C3NR05479A.

Sun, T.Y., Bornhöft, N.A., Hungerbühler, K., Nowack, B., 2016. Dynamic probabilistic modeling of environmental emissions of engineered nanomaterials. Environ. Sci. Technol. 50, 4701–4711. https://doi.org/10.1021/acs.est.5b05828.

Sun, X., Sheng, Z., Liu, Y., 2013. Effects of silver nanoparticles on microbial community structure in activated sludge. Sci. Total Environ. 443, 828–835. https://doi.org/10.1016/j.scitotenv.2012.11.019.

Tan, J.M., Qiu, G., Ting, Y.P., 2015. Osmotic membrane bioreactor for municipal wastewater treatment and the effects of silver nanoparticles on system performance. J. Clean. Prod. 88, 146–151. https://doi.org/10.1016/j.jclepro.2014.03.037.

Telgmann, L., Metcalfe, C.D., Hintelmann, H., 2014. Rapid size characterization of silver nanoparticles by single particle ICP-MS and isotope dilution. J. Anal. At. Spectrom. 29, 1265–1272. https://doi.org/10.1039/c4ja00115j.

Tulve, N.S., Stefaniak, A.B., Vance, M.E., Rogers, K., Mwilu, S., LeBouf, R.F., Schwegler-Berry, D., Willis, R., Thomas, T.A., Marr, L.C., 2015. Characterization of silver nanoparticles in selected consumer products and its relevance for predicting children's potential exposures. Int. J. Hyg Environ. Health 218, 345–357. https://doi.org/10.1016/j.ijheh.2015.02.002.

Tuoriniemi, J., Cornelis, G., Hassellöv, M., 2012. Size discrimination and detection capabilities of single-particle ICPMS for environmental analysis of silver nanoparticles. Anal. Chem. 84, 3965–3972. https://doi.org/10.1021/ac203005r.

Tuoriniemi, J., Jürgens, M.D., Hassellöv, M., Cornelis, G., 2017. Size dependence of silver nanoparticle removal in a wastewater treatment plant mesocosm measured by FAST single particle ICP-MS. Environ. Sci. Nano 4, 1189–1197. https://doi.org/10.1039/c6en00650g.

van Loosdrecht, M.C., Nielsen, P.H., Lopez-Vazquez, C.M., Brdjanovic, D., 2016. Experimental Methods in Wastewater Treatment. https://doi.org/10.1017/CBO9781107415324.004.

Wang, H., Adeleye, A.S., Huang, Y., Li, F., Keller, A.A., 2015. Heteroaggregation of nanoparticles with biocolloids and geocolloids. Adv. Colloid Interface Sci. 226, 24–36. https://doi.org/10.1016/j.cis.2015.07.002.

Wang, P., Menzies, N.W., Dennis, P.G., Guo, J., Forstner, C., Sekine, R., Lombi, E., Kappen, P., Bertsch, P.M., Kopittke, P.M., 2016. Silver nanoparticles entering soils via the wastewater-sludge-soil pathway pose low risk to plants but elevated Cl concentrations increase Ag bioavailability. Environ. Sci. Technol. 50, 8274–8281. https://doi.org/10.1021/acs.est.6b01180.

Wimmer, A., Kalinnik, A., Schuster, M., 2018. New insights into the formation of silver-based nanoparticles under natural and semi-natural conditions. Water Res. 141, 227–234. https://doi.org/10.1016/j.watres.2018.05.015.

Yu, S.J., Yin, Y.G., Chao, J.B., Shen, M.H., Liu, J.F., 2014. Highly dynamic PVP-coated silver nanoparticles in aquatic environments: chemical and morphology change induced by oxidation of Ag^0 and reduction of Ag^+. Environ. Sci. Technol. 48, 403–411. https://doi.org/10.1021/es404334a.

Zhang, C., Hu, Z., Deng, B., 2016a. Silver nanoparticles in aquatic environments: physiochemical behavior and antimicrobial mechanisms. Water Res. 88, 403–427. https://doi.org/10.1016/j.watres.2015.10.025.

Zhang, C., Hu, Z., Li, P., Gajaraj, S., 2016b. Governing factors affecting the impacts of silver nanoparticles on wastewater treatment. Sci. Total Environ. 572, 852–873. https://doi.org/10.1016/j.scitotenv.2016.07.145.

Zheng, X., Wang, J., Chen, Y., Wei, Y., 2018. Comprehensive analysis of transcriptional and proteomic profiling reveals silver nanoparticles-induced toxicity to bacterial denitrification. J. Hazard Mater. 344, 291–298. https://doi.org/10.1016/j.jhazmat.2017.10.028.